role for PMN-ECM interactions in host defense against virulent organisms than was previously realized.

REFERENCES AND NOTES

1. J. D. Pollock *et al.*, *Nature Genet.* **9**, 202 (1995).
2. S. H. Jackson, J. I. Gallin, S. M. Holland, *J. Exp. Med.* **182**, 751 (1995).
3. F. P. Lindberg, H. D. Gresham, E. Schwarz, E. J. Brown, *J. Cell Biol.* **123**, 485 (1993).
4. F. P. Lindberg *et al.*, *J. Biol. Chem.* **269**, 1567 (1994).
5. E. J. Brown, L. Hooper, T. Ho, H. D. Gresham, *J. Cell Biol.* **111**, 2785 (1990).
6. M. I. Reinhold *et al.*, *J. Cell Sci.* **108**, 3419 (1995).
7. H. D. Gresham, J. L. Goodwin, P. M. Allen, D. C. Anderson, E. J. Brown, *J. Cell Biol.* **108**, 1935 (1989).
8. M.-J. Zhou and E. J. Brown, *J. Exp. Med.* **178**, 1165 (1993).
9. H. D. Gresham, S. P. Adams, E. J. Brown, *J. Biol. Chem.* **267**, 13895 (1992).
10. D. Cooper, F. P. Lindberg, J. R. Gamble, E. J. Brown, M. A. Vadas, *Proc. Natl. Acad. Sci. U.S.A.* **92**, 3978 (1995).
11. C. A. Parkos *et al.*, *J. Cell Biol.* **132**, 437 (1996).
12. Peripheral blood leukocytes, splenocytes, and fibroblasts (*13*).
13. F. P. Lindberg *et al.*, unpublished data.
14. A cohort of 9 to 21 mice of each IAP genotype was tested for peripheral blood/hemoglobin, platelet count, and white blood cell (WBC) count at 38 days of age, and for WBC count and PMN count at both 9 to 11 weeks and 1 year of age. Counts were not significantly different between the genotypes. The PMN counts at 9 to 11 weeks were 1.30 ± 0.25, 1.70 ± 0.23, and 1.62 ± 0.18 cells per nanoliter (mean ± SEM), for $IAP^{+/+}$, $IAP^{+/-}$, and $IAP^{-/-}$ mice, respectively.
15. A. S. Cross *et al.*, *J. Exp. Med.* **169**, 2021 (1989).
16. J. H. Lowrance, F. X. O'Sullivan, T. E. Caver, W. Waegell, H. D. Gresham, *ibid.* **180**, 1693 (1994).
17. T. N. Mayadas, R. C. Johnson, H. Rayburn, R. O. Hynes, D. D. Wagner, *Cell* **74**, 541 (1993); M. L. Arbones *et al.*, *Immunity* **1**, 247 (1994); J. E. Sligh Jr. *et al.*, *Proc. Natl. Acad. Sci. U.S.A.* **90**, 8529 (1993); D. C. Bullard *et al.*, *J. Clin. Invest.* **95**, 1782 (1995).
18. G. Sarman, S. B. Shappell, E. O. Mason Jr., C. W. Smith, S. L. Kaplan, *J. Infect. Dis.* **172**, 1001 (1995).
19. E. J. Brown and F. P. Lindberg, in *Blood Cell Biochemistry: Macrophages and Related Cells*, J. A. Horton, Ed. (Plenum, New York, 1993), vol. 5, pp. 279–306.
20. H. D. Gresham *et al.*, *J. Clin. Invest.* **88**, 588 (1991).
21. A. G. Gao, F. P. Lindberg, M. B. Finn, S. D. Blystone, W. A. Frazier, *J. Biol. Chem.* **271**, 21 (1996).
22. H. D. Gresham, C. J. Ray, F. X. O'Sullivan, *J. Immunol.* **146**, 3911 (1991).
23. J. A. Griffin and F. M. Griffin Jr., *J. Exp. Med.* **150**, 653 (1979).
24. A cDNA for mouse IAP (*3*) was used to screen a 129/Sv genomic library (Stratagene, LaJolla, CA). An overlapping set of genomic clones encoding the 5′-end of the cDNA up to the first two-thirds of the multiply membrane-spanning domain was assembled. An IAP replacement construct was generated by inserting the *neo*^{r} gene from pPol2neobpA (gift from P. Soriano) into exon 2, which encodes the signal peptide cleavage site and entire IAP IgV domain. This construct was electroporated into AB2.1 embryonic stem cells [P. Soriano, C. Montgomery, R. Geske, A. Bradley, *Cell* **64**, 693 (1991); M. R. Kuehn, A. Bradley, E. J. Robertson, M. J. Evans, *Nature* **326**, 295 (1987); A. P. McMahon and A. Bradley, *Cell* **62**, 1073 (1990)]. Digestion with Sac I and hybridization with the probe indicated was used to identify homologous recombinants. Multiple clones were isolated that correctly targeted the IAP gene, and injection of one of these resulted in germline transmission.
25. Mice were tail bled, and washed erythrocytes stained first with mAb miap301 to mouse IAP, then with fluorescein isothiocyanate–labeled secondary antibody and analyzed by flow cytometry. As a negative control, an isotype-matched mAb to keyhole limpet hemocyanine (KLH) was used. Single-cell suspensions of mouse bone marrow (from femurs and tibiae) were similarly analyzed, except that staining was done in the presence of excess human IgG (1 mg/ml) to block Fc receptor interactions.
26. Erythrocyte ghosts were prepared from 1 ml of mouse blood by lysis and washing in 5 mM tris-HCl (pH 8.0) and 1 mM phenylmethylsulphonyl fluoride. Equivalent amounts of protein were solubilized in nonreducing SDS sample buffer, electrophoresed on a 10% SDS-polyacrylamide gel, and reacted with a 1/500 dilution of polyclonal rabbit antibody to IAP cytoplasmic tail (*3*) or to the IAP NH_2-terminus [raised to KLH-conjugated pyro-QLLFSNVNSIEFTSC (single letter amino acid code; pyro-Q, pyro-Gln; L, Leu; F, Phe; S, Ser; N, Asn; V, Val; I, Ile; E, Glu; C, Cys)] followed by washing, incubation with peroxidase-labeled goat antibody to rabbit IgG, and detection by enhanced chemoluminesence (Amersham, Arlington Heights, IL).
27. *Escherichia coli* O18:K1:H7 (*12*) was passaged twice in C57BL/6J mice before use. IAP-deficient (n = 4) or littermate controls (+/−; control) (n = 5) from mice back-crossed five generations onto C57BL/6J were inoculated intraperitoneally with 5×10^4 bacteria in 100 μl of pyrogen-free saline and observed as described (*16*). Mice back-crossed for eight generations yielded similar results (*13*).
28. IAP-deficient mice (n = 7) back-crossed for eight generations onto C57BL/6J and heterozygote littermate controls (n = 5) were challenged with 3×10^4 *E. coli* O18:K1:H17 (see Fig. 2). After 4 hours, mice were anesthetized and killed, and 5-ml peritoneal lavages in sterile saline obtained as described (*16*). Similarly, IAP-deficient (n = 6) and control (n = 5) mice were challenged with 4.3×10^4, and after 24 hours total cell counts, differential counts, and colony-forming units of *E. coli* were assessed and PMN counts were calculated.
29. Sheep red blood cells (RBCs) opsonized with murine IgG2b antibody to sheep RBCs were prepared and incubated with murine bone marrow PMNs after a brief centrifugation as described (*22*). After lysis of extracellular targets, RBCs phagocytosed per 100 PMNs (phagocytic index) were determined (*22*).
30. Microtiter plates were coated with 50 μl of eight-KGAGDVA-valent peptide (150 μg/ml) and eight-KGALEVA-valent peptide (150 μg/ml) as described (*8*). Then 2×10^5 murine bone marrow PMNs were added per well and hydrogen peroxide production assayed after 60 min with a scopoletin-based fluorescence assay (*8*).
31. Fluorescent latex beads (1.3 μm) were coated with eight-KGAGDVA-valent peptide or HSA as described (*9*). Next 3×10^5 murine bone marrow PMNs were incubated 15 min at room temperature in 100 μl of Hanks' balanced salt solution with catalase, 0.1 mM fMLP, and either normal rabbit IgG (30 μg/ml), rabbit IgG to human IAP (30 μg/ml), or rabbit antiserum to human placental Arg-Gly-Asp binding integrins (*30*) at a dilution of 1:200. Then 45 μl of beads were added and the mixture incubated for 30 min at 37°C. Cells were washed twice, and PMN-bound fluorescent beads were counted under an ultraviolet microscope and expressed as beads bound per 100 cells (attachment index).
32. C3bi-coated sheep erythrocytes (EC3bi) were made by incubating 200 μl of sheep erythrocytes coated with rabbit IgM to sheep erythrocytes, 190 μl of veronal-buffered saline with dextrose, Ca^{2+} and Mg^{2+} (VBS), and 10 μl of C5-deficient mouse serum (absorbed with sheep erythrocytes) for 1 hour at 37°C followed by washing and resuspension in 400 μl of VBS (*23*). Then 200,000 PMNs in 50 μl of VBS, 50 μl of 100 μM fMLP in VBS, and 15 μl of EC3bi were pelleted briefly and resuspended, followed by incubation at 37°C for 30 min. The number of EC3bi rosetted per 100 PMNs was determined microscopically. No EC3bi are ingested under these conditions (*23*).

33. We thank M. Williams, I. Lorenzo, and L. A. Hurley for technical assistance and P. Soriano for reagents. Supported by NIH grants GM38330 (E.J.B.), AI32177 (A.L.B.), GM15483 (D.C.B.), the Howard Hughes Medical Institute (F.P.L. and A.L.B.), the American Arthritis Foundation (E.J.B. and F.P.L.), the Research Service of the Department of Veterans Affairs (H.D.G.), and the Monsanto–Washington University Agreement.

5 July 1996; accepted 22 August 1996

Hyperresponsive B Cells in CD22-Deficient Mice

Theresa L. O'Keefe, Gareth T. Williams, Sarah L. Davies, Michael S. Neuberger*

CD22 is a surface glycoprotein of B lymphocytes that is rapidly phosphorylated on cytoplasmic tyrosines after antigen receptor cross-linking. Splenic B cells from mice with a disrupted CD22 gene were found to be hyperresponsive to receptor signaling: Heightened calcium fluxes and cell proliferation were obtained at lower ligand concentrations. The mice gave an augmented immune response, had an expanded peritoneal B-1 cell population, and contained increased serum titers of autoantibody. Thus, CD22 is a negative regulator of antigen receptor signaling whose onset of expression at the mature B cell stage may serve to raise the antigen concentration threshold required for B cell triggering.

Antigen interaction with the B cell antigen receptor (BCR) triggers a cascade of protein tyrosine phosphorylation, which, depending on the maturational state of the B cell and on the nature of additional signals, leads to activation or death (*1*). CD22 is a B cell–restricted glycoprotein with an extracellular domain that binds glycoconjugates containing α 2,6-linked sialic acid (*2*). It associates with BCR and, after BCR cross-linking, becomes phosphorylated on cytoplasmic tyrosines, which leads to the recruitment of the haematopoietic phosphatase SHP-1 (*3*–*5*).

To study the role of CD22 in BCR-induced signaling, we generated mice with a

Medical Research Council Laboratory of Molecular Biology, Hills Road, Cambridge CB2 2QH, UK.

*To whom correspondence should be addressed.

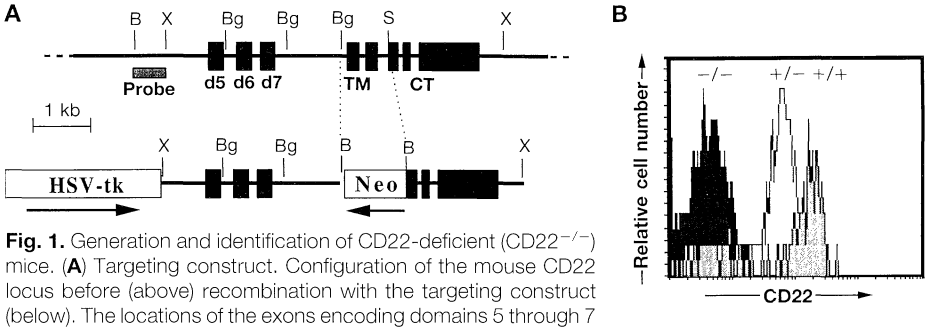

Fig. 1. Generation and identification of CD22-deficient ($CD22^{-/-}$) mice. (**A**) Targeting construct. Configuration of the mouse CD22 locus before (above) recombination with the targeting construct (below). The locations of the exons encoding domains 5 through 7 of the extracellular portion of CD22 as well as the transmembrane (TM) and cytoplasmic (CT) portions are indicated. B, Bam HI; Bg, Bgl II; S, Stu I; X, Xba I; HSV-tk, herpes simplex virus thymidine kinase gene; Neo, neomycin-resistance cassette. (**B**) Expression of CD22 on the surface of splenic B cells of $CD22^{-/-}$, $CD22^{+/+}$, and $CD22^{+/-}$ siblings was analyzed by flow cytometry with the Cy34.1.2 monoclonal antibody to CD22 (Lyb8.2; American Type Culture Collection) (*17*).

disrupted CD22 gene (*6*). Flow cytometry revealed that, although splenic B cells were present in near-normal abundance in CD22-deficient mice, CD22 was not detectable on their surface (Fig. 1). The expression of CD22 was also reduced on B cells from heterozygous $CD22^{+/-}$ animals.

The production and expansion of B-lineage precursors proceeded normally in CD22-deficient mice as revealed by analysis of the subpopulations in bone marrow (*7*); this is consistent with CD22 expression in normal mice being largely restricted to the mature B cell population (*8*). Splenic B cells were analyzed for a variety of cell surface markers (*9*), the most notable difference being that splenocytes from $CD22^{-/-}$ mice showed a depletion of IgM^{hi}-IgD^{hi} B cells with a shift toward an IgM^{lo}-IgD^{hi} phenotype (Fig. 2A). This is unlikely to reflect a requirement for CD22 for efficient surface transport of membrane immunoglobulin M (IgM), because peritoneal B cells from the CD22-deficient mice show high IgM expression (Fig. 2B). The shift toward an IgM^{lo}-IgD^{hi} phenotype parallels what has been observed in B cells carrying an anti–hen egg lysozyme (HEL) immunoglobulin transgene that have developed in the presence of the HEL ligand (*10*); it contrasts with the shift toward an IgM^{hi}-IgD^{hi} phenotype in the hyporesponsive B cells of CD45-deficient mice (*11*). We favor the hypothesis that this shift in the CD22-deficient animals reflects an augmented, possibly ligand-induced, maturational event due to the hyperresponsiveness of their B lymphocytes.

Experiments with antibodies to CD22 have revealed that CD22 can mediate signal transduction in B cells, although reports differ as to whether the presence of CD22 serves to augment or to inhibit signals delivered from BCR (*4*, *12*). Splenic B cells from CD22-deficient mice were considerably more sensitive to membrane IgM ligation than those from wild-type siblings; not only was a calcium flux achieved with lower concentrations of $F(ab')_2$ goat antiserum to mouse μ chain (anti-μ) (and similarly, of anti-δ), but the size of the spike was also larger (Fig. 3A). This at least in part reflects increased calcium release from internal stores (Fig. 3B). The CD22-deficient B cells also manifested increased sensitivity to BCR ligation by a monoclonal anti-μ as judged by proliferative responses and by up-regulation of the CD86 co-stimulatory molecule (Fig. 3, C to E). [The differences in proliferation of normal and CD22-deficient B cells induced by $F(ab')_2$ goat anti-μ was less evident, presumably because of the greater cross-linking effected.]

Signals initiated at the antigen receptor are not only needed for B cell maturation but are likely required for B cell maintenance. We therefore asked whether the loss of CD22 affected the size of the long-lived B cell pool. The peritoneal B-1 cell population [identified by its IgM^{hi}, IgD^{lo}, and $CD43^{+}$ phenotype (*13*)] is doubled in $CD22^{-/-}$ mice (Fig. 2B).

Monitoring antibody production after challenge with a T cell–dependent antigen revealed that the CD22-deficient mice gave augmented responses (Fig. 4A). Increased activation of B cells was also observed in the absence of specific immunization in that a higher proportion of B cells in the Peyer's patches of CD22-deficient mice exhibited a germinal center phenotype (Fig. 2C). Even in 7-week-old mice, the B cells from Peyer's patch germinal centers of CD22-deficient animals had accumulated multiple somatic mutations in their immunoglobulin genes (*14*).

Unimmunized CD22-deficient mice exhibited elevated concentrations of serum IgM, whereas the titers of the other isotypes were not significantly altered (Fig. 4B). Although the animals showed no significant incidence of autoimmune disease by 5 months of age, we noted that they often yielded serum titers of antibodies to DNA as judged by perinuclear staining of Hep-2 cells. Enzyme-linked immunosorbent assay (ELISA) confirmed the presence of increased titers of antibody to double-stranded (ds) DNA and antibody to dsDNA-histone complex (Fig. 4, C and D).

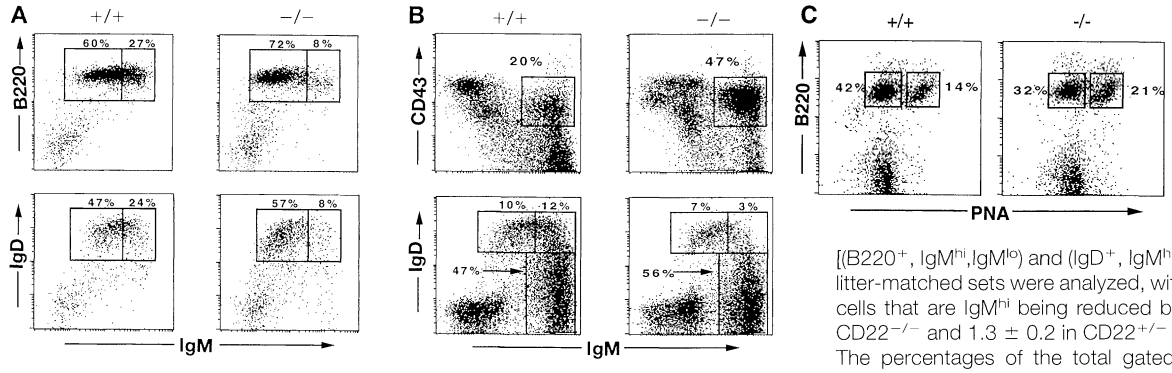

Fig. 2. Representative flow cytometric analysis of lymphocyte populations in CD22 homozygous mutant (−/−) and wild-type (+/+) littermates. (**A**) Spleen. The percentages of the total gated splenocytes falling within the boxed areas [($B220^{+}$, IgM^{hi},IgM^{lo}) and (IgD^{+}, IgM^{hi}, IgM^{lo})] are indicated. Five litter-matched sets were analyzed, with the proportion of $B220^{+}$ cells that are IgM^{hi} being reduced by a factor of 3.6 ± 1.8 in $CD22^{-/-}$ and 1.3 ± 0.2 in $CD22^{+/-}$ mice (*18*). (**B**) Peritoneum. The percentages of the total gated peritoneal cells that are $CD43^{+}$, IgM^{+} are indicated. Compared with wild-type littermates, the $CD22^{-/-}$ mice (n = 5) revealed a (2 ± 0.48)–fold increase in the proportion of peritoneal IgM^{+} cells that were $CD43^{+}$. (**C**) Peyer's patches. The percentages of the total gated Peyer's patch cells that were $B220^{+}$ and stained brightly or dully with peanut agglutinin (PNA) are indicated. The proportion of $B220^{+}$ cells that exhibited a PNA^{hi} phenotype was increased by a factor of 1.53 ± 0.21 in the $CD22^{-/-}$ mice (n = 4).

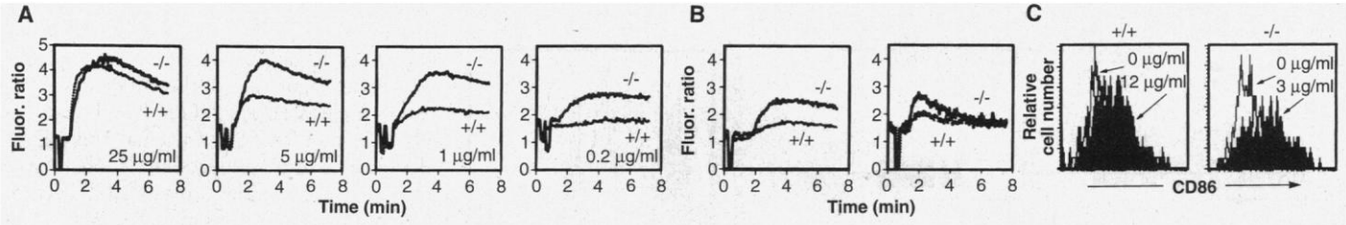

Fig. 3. In vitro responses of splenic B cells from CD22-deficient mice compared with those of normal littermates. (**A**) Changes in intracellular calcium concentrations ($[Ca^{2+}]_i$) as a consequence of BCR cross-linking with various concentrations (indicated) of $F(ab')_2$ goat anti-μ, with $[Ca^{2+}]_i$ represented as the ratio of indo-1 fluorescence at 395 nm to that at 530 nm (*19*). The results are averaged and are representative of all six pairs of $CD22^{-/-}$ and $CD22^{+/+}$ mice analyzed. (**B**) Changes in $[Ca^{2+}]_i$ after incubation with goat antiserum to mouse δ chain (0.2 μg/ml) (left panel) or $F(ab')_2$ goat antiserum to mouse μ chain (5 μg/ml) in the presence 1.8 mM EGTA (right panel). (**C**) Up-regulation of CD86 (B7-2) expression. After 24-hour incubation with monoclonal antibody (mAb) b-7-6 to mouse μ chain, normal B cells showed significant CD86 up-regulation only with concentrations of mAb b-7-6 ≥ 12 μg/ml, whereas CD22-deficient B cells showed clear CD86 up-regulation with a concentration of 3 μg/ml. (**D**) Proliferative responses (± SEM) induced by incubation with various concentrations of mitogenic mAb b-7-6 alone or with interleukin-4 (IL-4) (500 U/ml, Genzyme) were monitored in spleen cells from CD22-deficient mice (solid bars) and wild-type littermates (shaded) (*20*). Proliferative responses were also measured to (**E**) lipopolysaccharide (LPS) (bar sets 1 to 3; 0.016, 2, and 50 μl/ml, respectively) and anti-CD40 supernatant plus IL-4 (bar set 4). (**F**) Tyrosine phosphorylation of cellular proteins was analyzed at 0, 1, and 5 min after the addition of $F(ab')_2$ goat anti-μ (10 μg/ml) to suspensions of Histopaque-purified splenocytes from $CD22^{-/-}$ and wild-type littermates. Tyrosine-phosphorylated proteins were detected with mAb 4G10 to phosphotyrosine (Upstate Biotechnology) on protein immunoblots of whole-cell extracts. The migration of CD22 is indicated by an arrow, that of a 65-kD pair of major BCR-induced phosphorylation targets by an asterisk.

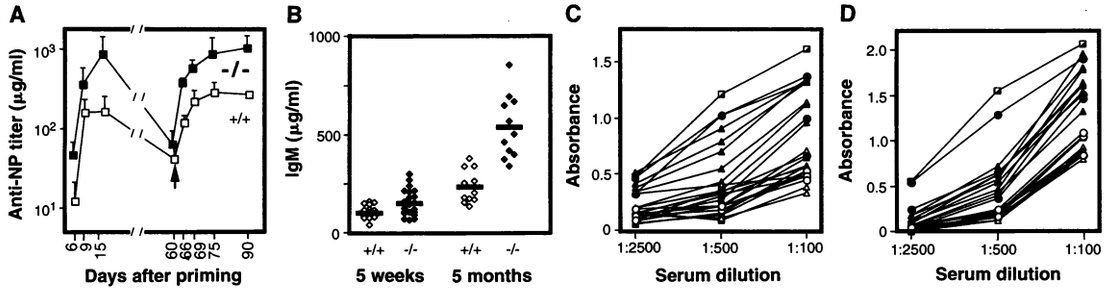

Fig. 4. Serum Ig titers. (**A**) Mean titers (± SEM) of λ-bearing 4(hydroxy-3-nitrophenyl)acetyl (NP)–specific antibody in sera from CD22-deficient (filled symbols; unimmunized titer was 1.1 ± 0.6 μg/ml) and wild-type (open symbols; unimmunized titer was 0.6 ± 0.3 μg/ml) mice at various times after intraperitoneal immunization with 50 μg of alum-precipitated NP_{17}-chicken γ-globulin. Similar results were obtained on measuring total IgG1 anti-NP titers. Animals were immunized on day 0 and boosted on day 60 (arrow). (**B**) Serum IgM concentrations in unimmunized mice were determined by ELISA with reagents and protocols from Pharmingen. (**C**) Titers of antibodies to dsDNA and (**D**) antibodies to DNA-histone complex were determined by ELISA (*21*) and developed with biotinylated anti–mouse κ. Sera were from CD22-deficient mice (filled symbols), wild-type litter mates (open symbols), MRL/lpr control serum (half-filled squares). The mice were 5 months old and from C57BL/6 breedings (circles) or 4 months old and from BALB/c breedings (triangles). The autoantibodies were predominantly of the IgM class, although elevated titers of IgG1 to dsDNA were also noted in some animals.

These experiments reveal CD22 as a negative regulator of BCR signaling. The mechanism of this negative regulation could well lie in the recruitment of SHP-1 by CD22 to the antigen-receptor complex (*4*, *5*). Indeed, SHP-1–deficient *viable motheaten* (me^v) mice also give exaggerated calcium responses on BCR triggering as well as show severe autoimmune disease, dramatically increased serum IgM concentrations, and an expanded B-1 population (*15*). The phenotype of CD22-deficient B cells contrasts with the hyporesponsiveness of B cells from mice lacking CD45 (*11*, *16*), suggesting that the CD45 phosphatase and CD22-associated SHP-1 act on distinct phosphotyrosines in the antigen-receptor signaling cascade. Indeed, the absence of CD22 does not appear to affect the kinetics of total cellular protein tyrosine phosphorylation induced by antigen receptor cross-linking (Fig. 3F), but this clearly does not exclude altered phosphorylation kinetics of individual components in the signaling cascade.

Our results, taken together with the developmental pattern of CD22 expression, support the idea that CD22 has a role in increasing the threshold of sensitivity to antigen that accompanies the differentiation of an immature B cell (which is sensitive to tolerization by low-affinity self-antigen) into a mature B cell that awaits triggering by exogenous antigen.

REFERENCES AND NOTES

1. M. R. Gold, D. A. Law, A. L. DeFranco, *Nature* **345**, 810 (1990); M. A. Campbell and B. M. Sefton, *EMBO J.* **9**, 2125 (1990); J. C. Cambier, C. M. Pleiman, M. R. Clark, *Annu. Rev. Immunol.* **12**, 457 (1994); K. Rajewsky, *Nature* **381**, 751 (1996).
2. B. Dörken *et al.*, *J. Immunol.* **136**, 4470 (1986); L. D. Powell, D. Sgroi, E. R. Sjoberg, I. Stamenkovic, A. Varki, *J. Biol. Chem.* **268**, 7019 (1993); C.-L. Law, S. P. Sidorenko, E. A. Clark, *Immunol. Today* **15**, 442 (1994).
3. R. J. Schulte, M. A. Campbell, W. H. Fischer, B. M. Sefton, *Science* **258**, 1001 (1992); C. J. G. Peaker and M. S. Neuberger, *Eur. J. Immunol.* **23**, 1358 (1993); C. LePrince, K. E. Draves, R. L. Geahlen, J. A. Ledbetter, E. A. Clark, *Proc. Natl. Acad. Sci. U.S.A.* **90**, 3236 (1993); G. T. Williams, C. J. G. Peaker, K. J. Patel, M. S. Neuberger, *ibid.* **91**, 474 (1994).
4. G. M. Doody *et al.*, *Science* **269**, 242 (1995).
5. M. A. Campbell and N. R. Klinman, *Eur. J. Immunol.*

25, 1573 (1995); G. Pani, M. Kozlowski, J. C. Cambier, G. B. Mills, K. A. Siminovitch, *J. Exp. Med.* **181**, 2077 (1995); C.-L. Law *et al.*, *ibid.* **183**, 547 (1996).
6. The CD22 gene was isolated from a phage λ2001 library prepared from 129 mouse DNA (gift from A. Smith). The Bgl II–Stu I fragment spanning the transmembrane exon was replaced by a neomycin-resistance (*neo*^{r}) cassette, and the HSV-*tk* gene was appended at the 5′ end of the construct to allow selection against random integration [K. R. Thomas and M. R. Capecchi, *Cell* **51**, 503 (1987); A. J. H. Smith *et al. Nature Genet.* **9**, 376 (1995)]. Embryonic stem (ES) cell line CCB (gift of M. Evans and obtained through A. Smith) was transfected with the targeting construct by electroporation. Southern blot analysis of Bam HI–digested DNA with the probe indicated in Fig. 1A yielded a 12.6-kb band for the wild-type gene and a 3.6-kb band for the targeted allele. One-sixth of the *neo*^{r} clones analyzed carried targeted integrations. Two of the targeted ES clones were used to establish chimeric mice by injection into C57BL/6 blastocysts, and germline transmission was obtained on further crossing with both C57BL/6 and BALB/c females.
7. B-lineage cells in bone marrow of CD22-deficient mice and control littermates were compared by flow cytometry for expression of IgM, CD45 (B220), CD19, and CD43.
8. L. D. Erikson, L. T. Tygrett, S. K. Bhatia, K. H. Grabstein, T. J. Waldschmidt, *Int. Immunol.* **8**, 1121 (1996).
9. Flow cytometric analyses were performed on 9- to 10-week-old CD22$^{-/-}$ mice and CD22$^{+/+}$ littermates generated from breeding the F_1 generation from a 129 × C57BL/6 cross. Single-cell suspensions were stained with fluorescein isothiocyanate (FITC)–conjugated goat antibody to mouse IgM (anti-IgM), phycoerythrin (PE)-conjugated anti–mouse IgD (Southern Biotechnology), FITC-conjugated peanut agglutinin (PNA) (Sigma), PE-conjugated anti-CD45R(B220) (RA3-6B2, Gibco BRL), or biotinylated anti-CD43 (S7, Pharmingen). Biotinylated antibodies were revealed with Red670-conjugated streptavidin and analyses performed on a FACScan, gating on lymphocytes by scatter. A more limited study from 129 × BALB/c breedings gave similar results to those shown in Fig. 2. With respect to other B cell surface markers examined (CD19, CD21/CD35, CD23, CD43, CD62L, CD69, CD86, and cell size), no major consistent changes were observed between splenic B cells of normal and CD22$^{-/-}$ animals.
10. C. C. Goodnow, J. Crosbie, H. Jorgensen, R. A. Brink, A. Basten, *Nature* **342**, 385 (1989).
11. K. E. Byth *et al.*, *J. Exp. Med.* **183**, 1707 (1996).
12. A. Pezzutto, B. Dörken, G. Moldenhauer, E. A. Clark, *J. Immunol.* **138**, 98 (1987); A. Pezzutto, P. S. Rabinovitch, B. Dörken, G. Moldenhauer, E. A. Clark, *ibid.* **140**, 1791 (1988); N. Chaouchi, A. Vazquez, P. Galanaud, C. Leprince, *ibid.* **154**, 3096 (1995); J. Tuscano, P. Engel, T. F. Tedder, J. H. Kehrl, *Blood* **87**, 4723 (1996); J. M. Tuscano, P. Engel, T. F. Tedder, A. Agarwal, J. H. Kehrl, *Eur. J. Immunol.* **26**, 1246 (1996).
13. S. M. Wells, A. B. Kantor, A. M. Stall, *J. Immunol.* **153**, 5503 (1994).
14. N. Klix and M. S. Neuberger, unpublished observations.
15. J. G. Cyster and C. C. Goodnow, *Immunity* **2**, 13 (1995); L. D. Shultz and M. C. Green, *J. Immunol.* **116**, 936 (1976); C. L. Sidman, L. D. Schultz, R. R. Hardy, K. Hayakawa, L. A. Herzenberg, *Science* **232**, 1423 (1986).
16. T. Benatar *et al.*, *J. Exp. Med.* **183**, 329 (1996); J. G. Cyster *et al.*, *Nature* **381**, 325 (1996).
17. F. W. Symington, B. Subbarao, D. E. Mosier, J. Sprent, *Immunogenetics* **16**, 381 (1982).
18. T. L. O'Keefe, G. T. Williams, S. L. Davies, M. S. Neuberger, unpublished observations.
19. Changes in intracellular calcium concentrations ($[Ca^{2+}]_i$) as a consequence of BCR cross-linking with various concentrations of $F(ab')_2$ goat anti-μ (Jackson) or goat antiserum to mouse δ chain (Nordic Immunological) were measured on indo-1–treated splenic lymphocytes that had been purified by banding on Histopaque (Sigma). T cells and activated lymphocytes were excluded by co-staining with biotinylated anti-CD43 and PE-streptavidin. The $[Ca^{2+}]_i$ was monitored with a fluorescence-activated cell sorting (FACS) flow cytometer and LYSIS II software (Beckton Dickinson) by measuring changes in the ratio of indo-1 emissions at 395 and 530 nm in real time.
20. Cells (2×10^5 cells in 0.2 ml) were incubated in triplicate samples with the indicated concentration of mAb b-7-6 to μ chain or lipopolysaccharide for 48 hours before a 16-hour incubation with 0.5 μCi of [^{3}H]thymidine, after which the radioactivity incorporated into macromolecules was measured. Similar results were obtained with three sets of CD22-deficient and normal mice. The mAb b-7-6 [M. H. Julius, C. H. Heusser, K.-U. Hartmann, *Eur. J. Immunol.* **14**, 753 (1984)] was a gift from M. Holman and G. Klaus.
21. C. Mohan, Y. Shi, J. D. Laman, S. K. Datta, *J. Immunol.* **154**, 1470 (1995).
22. We thank T. Rabbitts, A. Warren, and A. Smith for advice on ES cell culture; T. Langford and G. King for animal handling; A. Riddell and R. Hicks for performing flow cytometry analyses, M. C. Lamers and E. A. Clark for exchanging information before publication; and S. Bell, P. Dempsey, D. Fearon, A. MacKenzie, and members of our laboratory for advice and discussions. T.O'K. received a fellowship from Human Frontier Science Program Organization and S.L.D. and T.O'K. were also supported by an International Research Scholars award from Howard Hughes Medical Institute to M.S.N.

6 September 1996; accepted 4 October 1996

Visual Pigment Gene Structure and the Severity of Color Vision Defects

Jay Neitz,* Maureen Neitz, Pamela M. Kainz

Rearrangements of the visual pigment genes are associated with defective color vision and with differences between types of red-green color blindness. Among individuals within the most common category of defective color vision, deuteranomaly, there is a large variation in the severity of color vision loss. An examination of specific photopigment gene sites responsible for tuning photopigment absorption spectra revealed differences that predict these variations in the color defect. The results indicate that the severity of the defect in deuteranomalous color vision depends on the degree of similarity among the residual photopigments that serve vision in the color-anomalous eye.

Predicting the severity of a deficit from examination of a person's genetic makeup may prove to be particularly challenging for disorders that involve the nervous system and manifest themselves primarily as differences in behavior. Nonetheless, here is an example: a class of human color vision defect in which differences among the genes predict the severity of color vision loss. Deuteranomaly is the most common inherited color vision defect, affecting more than 1 in every 20 men in the United States. The condition arises from the absence of one of the cone photopigments, the normal pigment that is sensitive to middle wavelengths (M). Even though deuteranomalous individuals are missing normal M photopigment function, they retain varying degrees of trichromatic color vision, which is based on a pigment that is sensitive to short wavelengths plus two narrowly separated photopigments that absorb in the long-wavelength (L) region of the spectrum.

In this study, 16 young men were identified as deuteranomalous on the basis of a standard color matching test for red-green color vision defects—the Rayleigh match. In this test, the person is asked to mix together a red and a green light in a proportion that exactly matches the appearance of a monochromatic yellow light, as has been previously described (*1*). A deuteranomalous person chooses a much higher proportion of green light in the mixture than does a person with normal color vision. This color-matching test also distinguishes deuteranomalous trichromats from dichromats [as was done in (*2*)], who have only two cone photopigments and thus suffer the most severe of the common red-green color defects. Once we differentiated deuteranomalous men from men with normal color vision and from dichromats by means of the Rayleigh match, we assayed the severity of the color vision impairment using the American Optical, Hardy, Rand and Rittler (AO-HRR) pseudoisochromatic plates for color vision testing. From the complete set of plates included in the test, we used a series of six test figures designed for grading deutan color defects (Fig. 1A). Each design in this sequence is composed of a reddish-colored symbol on a background of gray dots. Each symbol in the progression is more intensely colored than the last.

The deuteranomalous participants varied enormously in their performance on this test. Although all 16 men had been classified as deuteranomalous in the color-matching test, a subset of these participants

Department of Cellular Biology and Anatomy and Department of Ophthalmology, Medical College of Wisconsin, 8701 Watertown Plank Road, Milwaukee, WI 53226, USA.

*To whom correspondence should be addressed.